PHILOSOPHICAL MAGAZINE B, 1999, VOL. 79, NO. 10, 1519–1530

Local structure of nanoporous carbons

V. PETKOV, R. G. DIFRANCESCO, S. J. L. BILLINGE†

Department of Physics and Astronomy and Center for Fundamental Materials Research, Michigan State University, East Lansing, Michigan 48824-1116, USA

M. ACHARYA and H. C. FOLEY

Center for Catalytic Science and Technology, Department of Chemical Engineering, University of Delaware, Newark, Delaware 19716, USA

[*Received 23 April 1999 and accepted 30 April 1999*]

ABSTRACT

The local atomic structure of nanoporous carbons produced by pyrolysis of poly(furfuryl alcohol) at various temperatures has been studied using neutron diffraction. Atomic pair distribution functions (PDFs) were obtained from the neutron data. Structure models have been fitted to the PDFs to understand the fine features of atomic ordering. It has been found that carbons produced at 800 and 1200°C are made of stacked graphene sheets, that are more or less curved. The 400°C-processed carbon has a heavily distorted nonplanar structure. For each sample we have determined the extent of the structural coherence, the average density within the structurally coherent regions and the proportion of carbon atoms, which are trigonally coordinated. We have also produced microscopic models for the local structure of the nanoporous carbons investigated.

§ 1. INTRODUCTION

There is considerable interest in using nanoporous carbon (NPC) in adsorptive separations and catalysis applications because of the large atomic-scale surface area (Suzuki 1990). The small pore sizes in these materials also allow some discrimination between molecules based on their size and shape (LaCava *et al.* 1989; Moyer *et al.* 1994). One approach for producing NPC is to pyrolyse hydrocarbons in an inert atmosphere at a high temperature (Juntgen *et al.* 1981). This produces carbon with favourable adsorptive and molecular sieving properties (Kane *et al.* 1996). There is, however, little that can be done to control the atomic structure or microstructure, other than by changing the process conditions. It is seemingly serendipitous that the resulting carbon is nanoporous with regular pores of approximately 4–5 Å diameter. In fact, the regular nanoporosity comes about because this material is structurally disordered on the nanometre length scale, in contrast with pure graphite for example. This makes it difficult to characterize the local atomic structure of NPC. Powder diffraction patterns contain weak diffuse scattering, and transmission electron microscopy images give patterns with tortuous arrangements of dark and light lines (Kane

† Author for correspondence: Email: billinge@pd.msu.edu.

Philosophical Magazine B ISSN 0141–8637 print/ISSN 1463–6417 online
http://www.tandf.co.uk/JNLS/phb.htm
http://www.taylorandfrancis.com/JNLS/phb.htm

et al. 1996; Acharaya *et al.* 1999). These are generally interpreted as coming from bent graphitic planes. Auxiliary structural information can be obtained from indirect methods such as helium pycnometry (skeletal density), nuclear magnetic resonance sp^2, sp^3-type carbon and other bonding defects) and elemental analysis (loss of heteroatoms such as hydrogen). It is clearly important to be able to characterize the structure of these materials on nanometre length scales if we are to differentiate between samples produced differently and ultimately to improve the absorptive characteristics through design.

We have carried out a thorough structural study on a set of three samples of pyrolized poly(furfuryl alcohol) (PFA) which were produced at 400°C (P4), 800°C (P8) and 1200°C (P12) respectively in an inert atmosphere. The synthesis has been described in detail by Kane *et al.* (1996). First-principles modelling of the same materials has also been described in a companion paper (Acharaya *et al.* 1999). The present study involves both obtaining real-space atomic pair distribution functions (PDFs) from powder neutron diffraction experiments and structure modelling guided by the diffraction data. This approach to analyse the data is standard for disordered materials, such as liquids, gels and glasses (Warren 1990) and can be fruitfully applied to fine crystalline powders as well (Egami 1990). Because of the well defined local atomic order in the carbon materials studied here it was important to collect diffraction data to large values of momentum transfer, $Q = [4\pi \sin(\theta)]/\lambda$. This was done by taking the data at a spallation neutron source: the Intense Pulsed Neutron Source at Argonne National Laboratory. The resulting PDFs, denoted $G(r)$, show peaks which correspond to the probability of finding atomic neighbours separated by a distance r. These PDFs have been fitted with structure models to extract quantitative information about the local atomic ordering in the samples. The PDFs results were compared with data from helium pycnometry and transmission electron microscopy (TEM) images reported elsewhere (Kane *et al.* 1996, Acharaya *et al.* 1999).

§ 2. Experimental details

2.1. *Neutron pair distribution function measurements*

Data from the P12 sample were collected on the Special Environment Powder Diffractometer (SEPD) and for the P8 and P4 samples on the Glass, Liquid and Amorphous Diffractometer (GLAD). Samples were placed in an incoherently scattering cylindrical vanadium can with diameter 0.5 cm and height 6 cm. The cans were filled with loosely packed powder. Data were collected in the time-of-flight mode at room temperature for approximately 4 h on SEPD and 8 h on GLAD. In addition, background data sets were measured with an empty diffractometer and an empty can respectively. Finally, an incoherently scattering vanadium rod was measured to correct for spectral and detector efficiency effects. The data were corrected for sample absorption, multiple scattering, inelasticity effects and backgrounds. The data were normalized by the incident flux and by the number of scatterers. From this corrected scattering intensity $I(Q)$, we obtained the so-called total structure factor $S(Q)$ according to

$$S(Q) = \frac{I(Q)}{\langle b \rangle^2} - \frac{\langle b^2 \rangle - \langle b \rangle^2}{\langle b \rangle^2}. \quad (1)$$

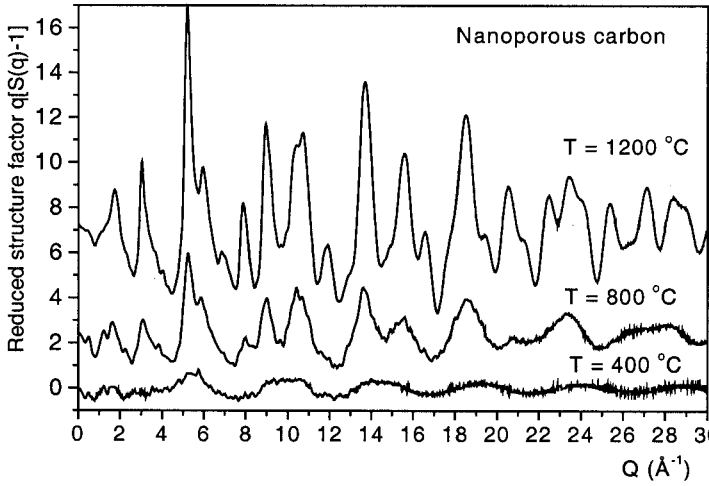

Figure 1. Reduced structure factors $i(Q)$ for samples P4, P8 and P12. The latter curves are offset vertically for clarity.

Here the b values are the scattering lengths for neutrons. The angular brackets indicate averages over isotopes and atom types in the sample, in this case simply carbon. The PDF is obtained from $S(Q)$ via a sine Fourier transformation:

$$G(r) = \frac{2}{\pi}\int_0^\infty i(Q)\,\sin(QR)\,dQ, \tag{2}$$

where the reduced structure factor $i(Q) = Q[S(Q) - 1]$ (Wagner 1978). The neutron diffraction data from the P4 sample had significant incoherent scattering from residual hydrogen, which complicated the derivation of the structure factor. To solve the problem the data were subjected to additional correction procedures based on the maximum-entropy method which has proved to be quite efficient in identifying and removing statistical and systematic errors from structure data of poorly ordered materials (Petkov and Danev 1998). The so-derived experimental $i(Q)$ values for the three samples are shown in figure 1. The corresponding PDFs are shown in figure 2.

2.2. *Density measurements*

Skeletal densities were measured using a Micrometrics 1320 helium pycnometer. Prior to making the measurements, the samples were backed at 120°C in air for 1 h and then transferred while warm to the pycnometer and evacuated with a roughening pump for 10 min. This was done to remove the residual moisture from the samples that could affect the accuracy of the density measurements. The following data for the density of the samples were obtained: $\rho(P4) = 1.38\,g\,cm^{-3}$, $\rho(P8) = 1.72\,g\,cm^{-3}$ and $\rho(P12) = 2.2\,g\,cm^{-3}$.

§ 3. Results

TEM images of P4, P8 and P12 samples show tortuous patterns of light and dark fringes (see figures 10–12 in Kane *et al.* (1996)). An intensity trace along a line in the image shows that the approximate periodicity of the fringes is 4.5 Å. This is compar-

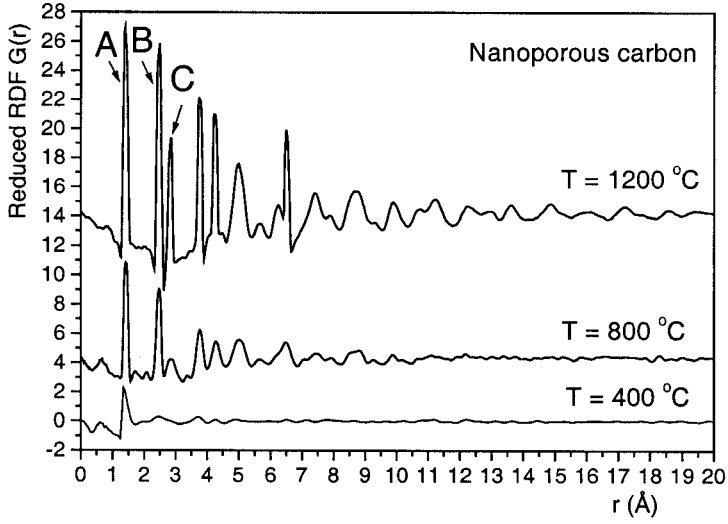

Figure 2. Atomic pair distribution functions in the form of the reduced radial distribution function, (RDF) $G(r)$ for samples P4, P8 and P12. The latter curves are offset vertically for clarity. A, B and C label the three distinct carbon–carbon distances occurring within the aromatic-type ring of graphite as depicted in figure 3.

able with but larger than the interlayer spacing of 3.4 Å in fully dense graphite (Wyckoff 1954). It thus makes sense to attribute the dark fringes to an oblique view of the ends of a single layer of graphite, that is of a single *graphene* sheet. It is clear that the sheets are fairly smoothly curved. As the processing temperature increases, the curvature of the sheets becomes less, the number of planes stacked above each other on average increases, and the size of the regions which can be recognized as smoothly curved graphite-like regions increases. We can quantify some of the TEM observations by referring to the experimental structure functions as follows. As can be seen in figure 1, the experimental structure factor for the P4 sample exhibits hardly detectable oscillations, as often found in heavily disordered materials. Thus the vague homogeneous pattern seen in the corresponding TEM image (see figure 10(*a*) of Kane *et al.* (1996)) is obviously due to the quite underdeveloped local atomic structure. Oscillations in I(Q) of the P8 sample are of much higher amplitude, which indicates the onset of an ordered microstructure for 800°C processing. The emerging domains of this microstructure contribute to the finely spotted pattern seen in the TEM image (see figure 10(*c*) of Kane *et al.* (1996)). With the 1200°C material P12, the structure factor already has sharp features, which come from atomic configurations ordered to length scales found with nanocrystalline materials. Correspondingly, one may interpret the sharp features in the TEM image (see figures 10(*d*) and 12 of Kane *et al.* (1996)) as being due to the presence of distinct nanocrystalline domains. The processes driven by the increase in treatment temperature apparently break the symmetry of the homogeneous and highly disorganized low temperature structure which seems to transform into an inhomogeneous semicrystalline atomic arrangement. This complex structural evolution, first suggested by TEM experiments (Kane *et al.* 1996), seems to be well verified by the present neutron diffraction patterns.

To reveal the fine features of the structural evolution that NPCs apparently undergo, we carefully examined the experimental PDFs. As can be seen in figure 2, the PDF for P4 sample has only one well defined first peak positioned at 1.41 Å, followed by a second broad peak at 2.6 Å. No discernible peaks are seen for real space distances longer than 5–6 Å, which is obviously the maximum extent of structural coherence in NPC produced at 400°C. For carbons obtained at 800 and 1200°C this extent turns out to be 10–12 and about 20 Å respectively.

To identify the basic structural units of the structurally coherent regions in P8 and P12 samples, we carefully considered the first few peaks in their PDFs. The first three peaks are positioned at real space distances of 1.41, 2.47 and 2.85 Å, respectively, which exactly match the in-plane carbon–carbon bond distances in the aromatic-type ring of graphite. For reference, such a ring is shown in figure 3. With the P12 sample the peaks are very well defined as can be seen in figure 2. By integrating the first peak in the experimental PDF it was found that the nearest-neighbour coordination number is 3.01 ± 0.15. This allows us to conclude that aromatic-type rings, such as that shown in figure 3, are the basic structural units in NPCs obtained at 1200°C. Also, the sheets forming the nanocrystalline domains observed in the TEM image (see figure 12 of Kane *et al.* (1996)) are likely to be built from such rings, that is the sheets are actually of a graphene type, as suggested above. As we discuss below, however, there is no evidence in the PDF that peaks come from interlayer atomic correlations. There is clearly significant turbostratic and positional disorder from one graphene sheet to the next and the sheets are not stacked in perfect registry. This is probably a natural consequence of the curvature and general disorder, which is evident in the TEM images (Kane *et al.* 1996). The loss of structural coherence beyond about 20 Å along the graphene sheet is also most probably due to the curvature of the sheets, and the distribution of curvatures in the sample, rather than from termination of sheet fragments.

With the P8 sample the situation is a slightly more complicated. The third-neighbour intraring distance (labelled C in figures 2 and 3) is broadened and the first coordination number turns out to be 2.6 ± 0.15. There is also a marked drop in intensity in the third-neighbour peak compared with that in P12 (figure 2, top curve). The third neighbour peak is present in six-membered carbon rings but not in five-fold rings. This peak also will be present in higher order rings (more than six

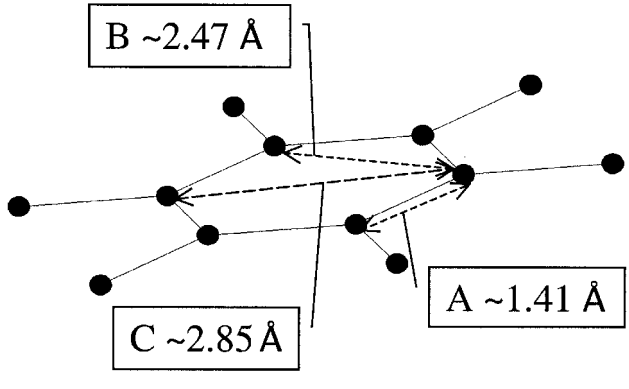

Figure 3. Carbon–carbon bond distances in an aromatic-type ring of graphite. The distances are labelled A, B and C for simplicity.

members) but will tend to appear at a different distance depending on the size of the ring. The fact that this peak is relatively weak and broadened is strong evidence that there is a significant proportion of non-hexagonal rings in the structure. The aromatic-type rings and, hence, the graphene sheets present here are somewhat defective. This is corroborated by the lower nearest-neighbour coordination measured. It is also consistent with the higher degree of sheet curvature seen in the TEM image (see figure 10 (*c*) of Kane *et al.* (1996)) and the related shorter range of structural coherence in the graphene sheet (10–12 Å) seen in the PDF and the lower density of this material.

The lack of well defined second- and third-neighbour intraring distances (labelled B and C in figures 2 and 3) in the PDF of P4 and the rather low first coordination number of 1.9 ± 0.2 clearly indicate that the aromatic-type rings, if any, are heavily distorted and defective in this rather disordered material. It is not a surprise then that no well defined sheet-like pattern is seen in the corresponding TEM image (see figure 10 (*a*) of Kane *et al.* (1996)). Also, the significant amount of residual hydrogen in the sample, evidenced by a strong incoherent scattering background in the neutron measurement, strongly suggests that in this case sheet fragments are small and terminated with hydrogen, in contrast with the samples synthesized at higher temperatures.

A distinct feature of all three experimental PDFs is that they have no peak at a real space distance of 3.4–3.5 Å (see figure 2) where the interlayer atomic correlations in graphite show up. Instead, the fourth peak in the experimental PDFs appears at 3.75 Å, which is the subsequent in-plane carbon–carbon bond distance in graphite (Wyckoff 1954). This observation shows that in P8 and P12 samples the graphene sheets are not stacked regularly even though they are seen to run in parallel in the TEM images (see figures 10 (*c*) and (*d*) of Kane *et al.* (1996)).

In general, both the experimental structure functions and the TEM images suggest that, on an atomic scale, P12 and P8 samples are made of almost perfect (P12) and defective and curved (P8) graphene sheets respectively, which are not spatially correlated. Based on similar although inferior neutron diffraction data, Mildner and Carpenter (1982) arrived at a similar conclusion for their nanophase carbon samples. Concerning sample P4, one may suggest that it is heavily disordered and does not seem to be built of aromatic-type structural units. The structural characteristics of NPCs just outlined were further refined and verified by fitting the experimental PDFs with appropriate structural models. It may be added that the present experimental structure functions $I(Q)$ and $G(R)$ are quite different from those obtained and discussed by Gaskel *et al.* (1992) and Li and Lannin (1990). The difference comes about from the different carbon samples studied, more graphitic in this case and certainly diamond like in their case.

§ 4. Modelling the local structure of nanoporous carbon

Structural modelling was carried out using a full-profile fitting least-squares approach described by Billinge (1998). This approach is similar to Rietveld refinement of crystalline powder diffraction since structural parameters such as atomic positions, thermal factors and site occupancies are refined. It is done by constructing an appropriate atomic configuration, calculating the respective model PDF and comparing it with the experimental PDF. Structural parameters in the model are then changed in such a way as to improve the agreement between the model calculated and experimental PDFs. Contrary to Rietveld refinement, which allows only

the determination of the long-range *average* structure of crystalline materials, the PDF-fitting approach allows the determination of both *local* atomic arrangements and intermediate range order on the nanometre length scale.

In accord with our preliminary analyses the following trial structure models were fitted to the experimental PDFs. The experimental PDF for the P12 sample was fitted with a structure model resembling a perfect graphene sheet. The structure model was based on a single unit cell of graphite and it was simulated to be a long-range structure by applying periodic boundary conditions. The unit-cell constants, atomic positions, atomic site occupancies and effective thermal factors were varied until the fit to the experimental data was optimized. A comparison between the final model and experimental PDFs is shown in figure 4. The quite good agreement seen was achieved without substantially modifying the atomic positions and occupancies in the starting atomic configuration, that is those in graphite. The only parameter changed was the temperature factor of carbon atoms in the out-of-plane (z) direction, where plane refers to the plane of the graphene sheet. This was artificially enlarged to remove well defined interlayer atomic correlations from the model whilse maintaining the microscopic density at the correct value. It ended an order of magnitude larger than the in-plane ((x, y) plane) temperature factors and so the complete lack of correlation between the neighbouring graphene sheets in the P12 material was effectively modelled. The gradual fall-off in structural coherence with increasing r was accounted for by multiplying the model PDF with a broad Gaussian function.

A single unit cell of graphite was the starting structure model for the P8 sample as well. Again periodic boundary conditions were applied and the model PDF was damped with a broad Gaussian function to account for the limited structural coherence (10–12 Å). The cell constants, atomic positions, occupancies and thermal factors were varied until the fit to the experimental PDF data converged. A comparison between the experimental and model PDFs is shown in figure 5. The agreement seen was achieved by moving the carbon atoms slightly away from their positions in the

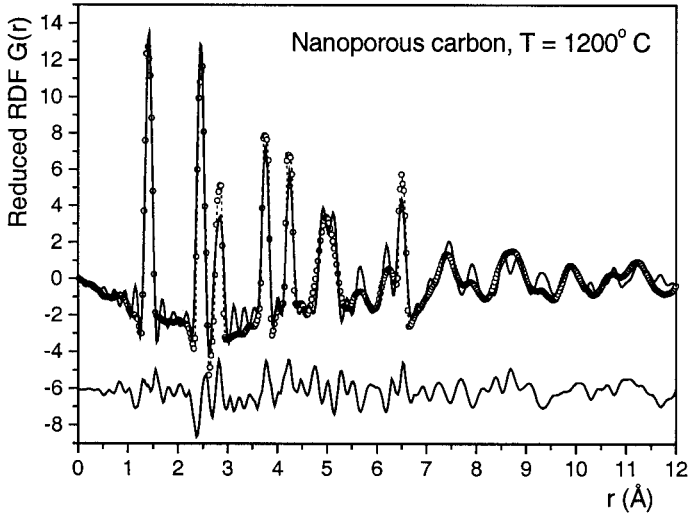

Figure 4. Comparison of the experimental PDF for the 1200°C sample (○) with the calculated PDF (———) derived from a perfect-graphene-sheet-based model. The residual difference is given as the lower curve.

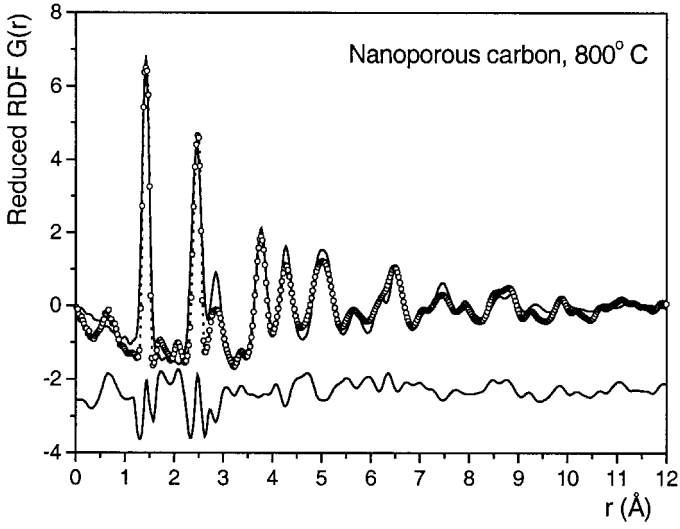

Figure 5. Comparison of the experimental PDF for the 800°C sample (○) with the calculated PDF (———) derived from a slightly-curved-graphene-sheet-type model. The residual difference is given in the lower curve.

graphite layers in a way that the structure became bent in the out-plane direction. In addition, the atomic site occupancies had to be reduced, which created some number of atomic vacancies. This accounts for the reduction in the number of nearest neighbours and the lower density. The loss in intensity in the third-neighbour peak, however, was not accounted for in this model. To account properly for this feature a network model with five- and seven-membered rings (and higher-order rings) would have to be constructed and this was not attempted here but has been done elsewhere (Acharya *et al.* 1999). Nonetheless, there is very satisfactory agreement between the model and the data. The two-dimensionality of the structure was again effectively modelled by bringing the temperature factors of carbon atoms in the out-of-plane direction to values an order of magnitude larger than those in the plane of graphene sheet.

Many more modifications on the starting structure model for the P4 sample (again a single unit cell of graphite) were necessary in order to obtain a reasonable agreement between the model and experimental PDFs. Carbon atoms were moved far away from their positions in the graphite lattice, their effective temperature factors required large values in all directions and, furthermore, a large number of atomic vacancies needed to be introduced. The modifications rendered the initially ordered structure model into a heavily disordered atomic configuration bearing only a slight resemblance with graphite. A comparison between the so-obtained model and experimental PDFs for the P4 sample is shown in figure 6.

The density of the atomically dense regions of the samples was determined from the PDF fits using model sensity = unit cell size/(number of atoms × occupancies). The values that we obtained in this way were 2.1 g cm^{-3} (P12), 1.8 g cm^{-3} (P8) and 1.5 g cm^{3} (P4), which turned out to be rather close to the skeletal densities obtained from helium pycnometry. This good agreement provides extra evidence in support of the reliability of the structure models constructed by the PDF approach.

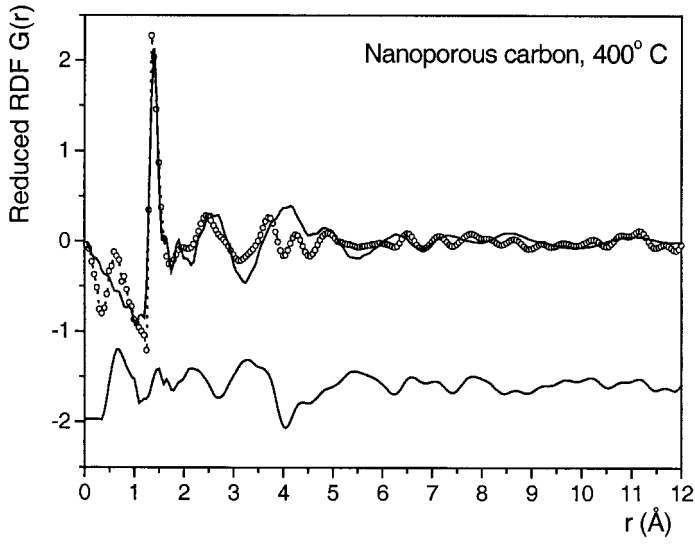

Figure 6. Comparison of the experimental PDF for the 400°C sample (○) with the calculated PDF (———) derived from a heavily disordered graphite-like atomic configuration. The residual difference is given as the lower curve.

§ 5. Discussion

The successful fitting of the PDF of the P12 sample with a structure model resembling a single graphene sheet shows that the NPCs obtained at 1200°C exhibit a two-dimensional local atomic order only. The structural coherence extends to approximately 20 Å where the oscillations in the experimental PDF completely fade away (see figure 2). Atomic order of such an extent should involve the presence of nanocrystalline domains with approximate size 40 Å, a value in good agreement with the TEM observations (Kane *et al.* 1996). Also, as the parameters of the refined structure model show, the graphene sheets forming the nanocrystalline domains in P12 sample are almost perfect (no vacancies) and not highly curved on a nanometre scale.

The results of the PDF fit suggest that carbons obtained at 800°C (P8) also exhibit a two-dimensional order only. The order extends to approximately 10–12 Å which limits the size of ordered structure regions (domains) to less than 24 Å. By contrast with the P12 sample, the graphene sheets in P8 sample are curved and defective. The curvature is considerable since it leads to a wide distribution of the third-neighbour carbon–carbon bonds in the aromatic-type rings of graphene as is demonstrated by the reduced amplitude and increased full width at half-maximum of the third peak (labelled C in figure 2) in the experimental PDF. The presence of defects reduces the density of the structurally coherent regions in the P8 sample to a value (1.9 g cm^{-3}) considerably lower than that (2.2 g cm^{-3}) in graphite.

The PDF modelling also showed that carbons obtained by PFA at 400°C are disordered to such an extent that domains of curved or flat graphene-like sheets are hardly recognizable. Since the first coordination number is 1.9 ± 0.2, aromatic-type rings may only be occasionally present in this material and, alternatively, it even may be perceived as an assembly of interconnected short chains of carbon atoms. This

peculiar and not quite planar atomic arrangement is very likely to have emerged when heteroatoms from the polymeric molecules of the precursor material, PFA have been driven out of the sample and little subsequent structure rearrangement has taken place owing to the relatively low temperature of pyrolysis (400°C only). This view is also supported by the significant buckling which had to be introduced in the model for the P4 sample, which was not needed to fit P8 and P12, suggesting that in P4 the carbon–carbon–carbon bonds are not coplanar (figure 7). The significant hydrogen content in the sample also supports the nonplanar structural motif for sample P4. The hydrogen atoms most probably are those that terminate the dangling bonds of the sheet fragments.

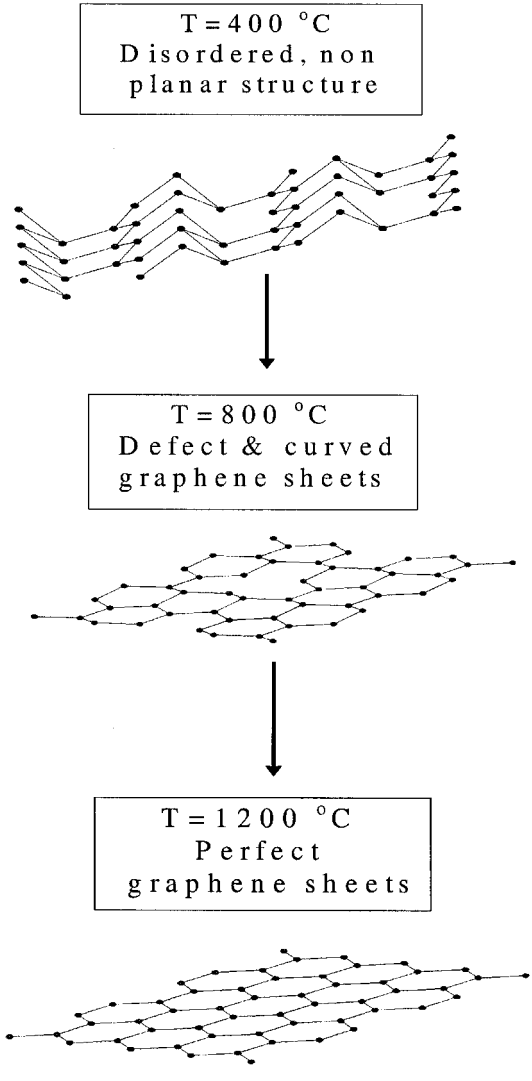

Figure 7. Example of the evolution of the local atomic structure of NPCs obtained by pyrolysis of PFA at 400, 800 and 1200°C. The atomic configurations shown resemble fragments of the model structures constructed by the PDF-fitting approach.

Summarizing, the structural evolution of NPCs may be described as follows: At a relatively low pyrolysis temperature (400°C) the NPCs produced have rather distorted and not quite planar atomic ordering which extends to 5–6 Å only. The average density is considerably lower than that of graphite and no more than 63% of carbon atoms, as estimated from the experimental first coordination number, are trigonally like coordinated. When the pyrolysis temperature increases to 800°C, the resulting NPC densifies, its local structure becomes more planar and the percentage of trigonally coordinated atoms increases to 86% as the experimental first coordination number shows. When the process of pyrolysis is carried out at a sufficiently high temperature (1200°C), all carbon atoms seem to acquire perfect trigonal coordination (the first coordination number is effectively three), graphene sheets are organized into extended nanocrystalline domains and the density approaches that of graphite. The local structure, however, lacks three-dimensional coherency and that is why it is still not that of graphite. The so-described structural evolution is schematically presented in figure 7. It is worth noting that Kane *et al.* (1996) found that carbons obtained at temperatures between 400°C and 800°C best differentiate between oxygen and nitrogen molecules. Based on the structural results just presented, one may then speculate that NPCs that are locally disordered but on the verge of showing graphite-like structural features are very likely to be the best candidates for application in adsorptive separations.

§ 6. Conclusion

Experimental PDFs and structure models fitted to them give the following consistent picture of the local atomic ordering of carbons obtained by pyrolysis of PFA. Carbon obtained at a relatively low temperature (400°C) is heavily distorted on an atomic scale and possesses a relatively open structure which resembles neither that of trigonally coordinated and layered graphite nor that of tetrahedrally coordinated diamond. Its local structure may be well approximated with an assembly of uncorrelated polymeric-like chains of carbon atoms. Carbons obtained at 800°C are made of curved and somewhat defective graphene sheets which are just starting to evolve into structurally coherent domains. Carbons obtained at 1200°C are made of stacks of uncorrelated graphene sheets forming nanocrystalline domains extended to about 40 Å.

Acknowledgements

S.J.L.B. would like to acknowledge funding support from the National Science Foundation through grant CHE-9633798 and from the Alfred P. Sloan Foundation. H.C.F. thanks the US Department of Energy, Basic Energy Sciences (BES) and the Du Pont Company for support of this research. The neutron diffraction experiments were carried out at the Intense Pulsed Neutron Source at Argonne National Laboratory. This facility is funded by the US Department of Energy, BES-Materials Science, under contract W-31-109-Eng-38.

References

Acharya, M., Strano, M.S., Matthews, J. P., Billinge, S. J. L., Petkov, V., Subramoney, S., and Foley, H. C., 1999, *Phil Mag.* B., **79**, 1499.

Billinge, S. J. L., 1998, *Local Structure From Diffraction*, edited by S. J. L. Billinge and M. F. Thorpe (New York: Plenum), p. 137.

Egami, T., 1990, *Mater. Trans. Japan Inst. Metal,* **31**, 163.

Gaskel, P. H., Saeed, A., Chieux, P., and McKenzie, D.R. 1992, *Phil. Mag.*, B, **66**, 155.
Juntgen, H., Knoblauch, K., and Harder, K. 1981, *Fuel,* **60**, 817.
Kane, S. M., Goellner, J. F., Foley, H. C., DiFrancesco, R., Billinge, S. J. L., and Allard, L. F. 1996, *Chem. Mater.,* **8**, 2159.
LaCava, A. I., Koss, V. A., and Wickens, D. 1989, *Gas Separation Purification,* **3**, 180.
Li, F., and Lannin, J. 1990, *Phys. Rev. Lett.,* **65**, 1905.
Mildner, D. F. R., and Carpenter, J. M. 1982, *J. non-crystalline Solids,* **47**, 391.
Moyer, J. D., Gaffney, T. R. Armor, J. N., and Coe, C. G. 1994, *Microporous Mater.,* **2**, 229.
Petkov, V., and Danev, R., 1998, *J. appl. Crystallogr.,* **31**, 609.
Suzuki, M., 1990, *Adsorption Engineering* (Amsterdam: Elsevier).
Wagner, C. N. J., 1978, *J. non-crystalline Solids,* **31**, 1.
Warren, B. E., 1990, *X-ray Diffraction* (New York: Dover Publications).
Wyckoff, R., 1954, *Crystal Structures* (New York: Wiley).